Primordial Black Holes and Scalar-induced Gravitational Waves in Sneutrino Hybrid Inflation

Adeela Afzal [a†], **Anish Ghoshal** [b‡], **Stephen F. King** [c*]

[a] *Department of Physics, Quaid-i-Azam University, Islamabad, 45320, Pakistan*
[b] *Institute of Theoretical Physics, Faculty of Physics, University of Warsaw, ul. Pasteura 5, 02-093 Warsaw, Poland*
[c] *School of Physics and Astronomy, University of Southampton, Southampton SO17 1BJ, United Kingdom*

E-mail: [†]adeelaafzal555@gmail.com, [‡]anish.ghoshal@fuw.edu.pl, [*]king@soton.ac.uk

Abstract. We investigate the possibility that primordial black holes (PBHs) can be formed from large curvature perturbations generated during the waterfall phase transition in a supersymmetric scenario where sneutrino is the inflaton in a hybrid inflationary framework. We obtain a spectral index ($n_s \simeq 0.966$), and a tensor-to-scalar ratio ($r \simeq 0.0056 - 10^{-11}$), consistent with the current Planck data satisfying PBH as dark matter (DM) and detectable Gravitational Wave (GW) signal. Our findings show that the mass of PBH and the peak in the GW spectrum is correlated with the right-handed (s)neutrino mass. We identify parameter space where PBHs can be the entire DM candidate of the universe (with mass $10^{-13}\,M_\odot$) or a fraction of it. This can be tested in future observatories, for example, with amplitude $\Omega_{\mathsf{GW}}h^2 \sim 10^{-9}$ and peak frequency $f \sim 0.1$ Hz in LISA and $\Omega_{\mathsf{GW}}h^2 \sim 10^{-11}$ and peak frequency of ~ 10 Hz in ET via second-order GW signals. We study two models of sneutrino inflation: Model-1 involves canonical sneutrino kinetic term which predicts the sub-Planckian mass parameter M, while the coupling between a gauge singlet and the waterfall field, β, needs to be quite large whereas, for the model-2 involving $\alpha-$attractor canonical sneutrino kinetic term, β can take a natural value. Estimating explicitly, we show that both models have mild fine-tuning. We also derive an analytical expression for the power spectrum in terms of the microphysics parameters of the model like (s)neutrino mass, etc. that fits well with the numerical results. The typical reheat temperature for both the models is around $10^7 - 10^8$ GeV suitable for non-thermal leptogenesis.

Contents

1 Introduction

Following recent remarkable data from cosmic microwave background radiation (CMBR) acquired by the Planck satellite, cosmic inflation has become the paradigm for early universe cosmology. Moreover, due to the vacuum energy scale during inflation being approximately 10^{14} GeV (largest allowed energy scale by CMB) is close to the expected Grand Unification scale and seesaw scale, such measurements are a pathway to directly probe into ultra-violate particle physics.

Alongside, the CMB scale and the physics during inflation, there has also been a great growing interest in the late stages of the inflationary paradigm, particularly the investigating scenarios where considerably large peaks in the amplitude of perturbations could be realized. This is because such peaks could lead to the formation of primordial black holes (PBHs) which has gained lots of interest after the observations of the supermassive [1, 2] and stellar-mass black hole (BH) merger events detected via observing gravitational wave (GW) in LIGO-VIRGO-KAGRA [3, 4]. Such large primordial density fluctuation could generate a stochastic gravitational wave background (SGWB) when PBHs are generated via the collapse of high-dense regions [5–7]. Typically, this requires the inflaton to go through a very flat potential during inflation (see ref. [8] for a recent review on PBHs) and involves some higher degrees of fine-tuning; see ref.[9] for details. This was first studied decades ago in ref. [10] in the context of a hybrid inflation scenario [11, 12]. It was recently shown that hybrid inflation naturally reduces the fine-tuning involved in producing PBH as dark matter (DM) [13, 14].

In this paper, we reconsider the possibility that the inflaton sector is responsible for generating the tiny neutrino masses required to explain several neutrino oscillation experiments. Heavy singlet neutrinos with scalar partners called sneutrinos with $10^{10} - 10^{15}$ GeV, lies in the range where the inflaton mass may lie. In this paper, we discuss two supersymmetric scenarios where the lightest heavy singlet (s)neutrino drives inflation. As we will see, this scenario constrains in interesting ways many of the 18 parameters of the minimal seesaw model for generating three non-zero light neutrino masses. This minimal (s)neutrino inflationary scenario can be rescued within the framework of hybrid inflation along with a successful neutrino oscillation data explanation. In terms of the early universe, this scenario provides a natural way to accommodate baryogenesis via leptogenesis due to sneutrino decay [15]. We will show that the mass of PBH and the peak in the GW spectrum is correlated with the right-handed (s)neutrino mass.

As previously demonstrated in the literature, the waterfall transition happening in the last stages of inflation, can have a flat potential to generate large curvature perturbations at small scales [16–18]. These large density perturbations, lead to a larger amplitude of curvature perturbations and eventually collapses into a PBH. As demonstrated in refs. [19, 20], this usually leads to the PBH overproduction of astrophysical size. However, this can be circumvented and the PBH abundance modulated with observable scalar-induced Gravitational Wave (SIGW) signals using a slightly modified waterfall field potential [21]. Since the crucial process of PBH generation estimates is subject to multiple significant uncertainties, we study it in less detail. However, we study in detail the characterization of the SGWB induced at the second order by the large curvature perturbations (at small length scales) during horizon reentry in the radiation-dominated era[1].

In a nutshell, we show that supersymmetric hybrid inflation involving neutrino mass could be tested via PBH and GW observations at energy scales beyond the TeV limit of collider physics. The flow of the paper is as follows: in section 2 we presented a toy model of hybrid inflation and the numerical framework for the power spectrum is given in section 3. The analytical calculations for the power spectrum are given in section 4. We analyze the toy model in a realistic supersymmetric framework in section 5. The PBH abundance and SIGWs are calculated in section 6 and section 7 respectively. We modify our model in terms of α-attractor framework in section 8 and present the fine-tuning estimate for both cases in section 9. We conclude in section 10.

2 *Model*-1: Toy Model Hybrid Inflation

Our focus in this paper is to study the footprints of supersymmetry in the SIGWs and PBHs. For this purpose, let us consider a toy model with hybrid inflationary potential. The critical point of instability, where the two scalar fields in the hybrid inflation become unstable, plays a crucial role in PBH production. The hybrid inflationary potential close to the critical point of instability can be written as

$$V = \Lambda \left(\left(1 - \frac{\psi^2}{M^2}\right)^2 + \frac{\phi - \phi_c}{m_1} - \frac{(\phi - \phi_c)^2}{m_2^2} + \frac{\phi^4 \psi^2}{M^2\, \phi_c^4} + \frac{\psi}{b} \right). \tag{2.1}$$

Here, ϕ is the inflaton field, ψ is the waterfall field, ϕ_c is the critical point below which the potential develops a tachyonic instability, forcing the field trajectories to reach one of the global minima, located at $\phi = 0$, $\psi = \pm M$, m_1, m_2 are the dimensionful mass parameters and Λ is the non-zero vacuum energy[2]. Usually, the hybrid inflation model predicts PBH overabundance [19]. We have added a linear term in the waterfall field that does not allow ψ to relax exactly at zero but slightly displace depending upon the sign. of the co-efficient of the linear term $1/b$. In this way, one can control the peak of the power spectrum and avoid the PBH overproduction A schematic picture of the model is shown in fig. 1.

[1]See ref. [22, 23] for other ways to generate PBH during hybrid inflation scenarios.

[2]The minimum of the whole potential is $V_{\rm min} = \pm\Lambda(M/b)$. Now, Λ is the inflation energy density scale because $H^2 = \Lambda/3$ as mentioned before eq. (4.3), however, b is not too small (in Table 1 and Fig. 3 we will see that $b \sim 10^9 m_{\rm Pl}$ and $M = 0.1\, m_{\rm Pl}$ (Table 1). This means that $V_{\rm min} \sim \pm 10^{-22} m_{\rm Pl}^4$. Although this is huge compared to the vacuum density of ΛCDM we can always adjust the unknown cosmological constant to cancel the vacuum density of the deeper minimum.

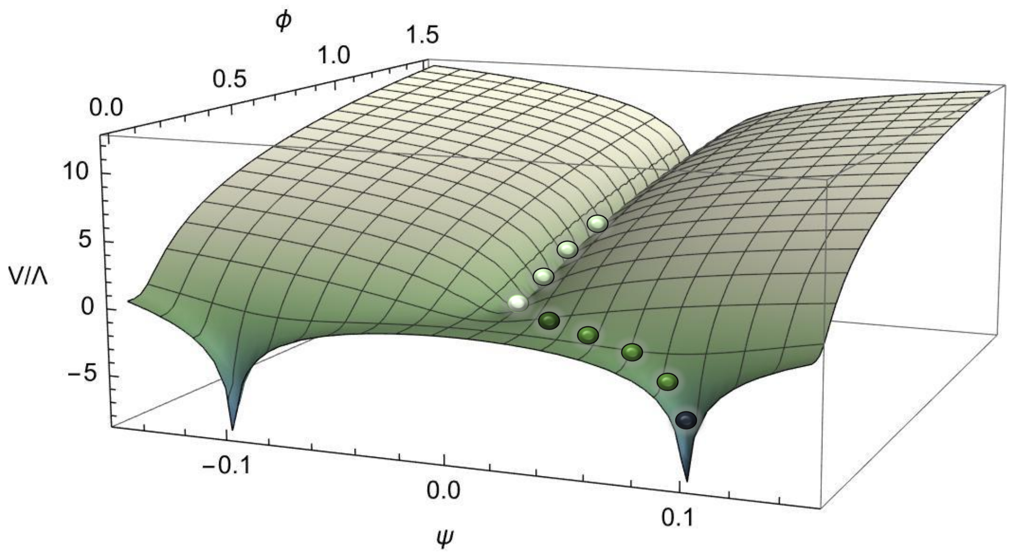

FIGURE 1: *A schematic picture of hybrid inflation potential given in eq. (2.1). The light green bullets show the inflationary trajectory of the inflaton ϕ, the white bullet is the critical point and the dark green bullets show the waterfall regime.*

The slow-roll parameters are given by, [24],

$$\epsilon_V = \frac{m_{\rm Pl}^2}{2}\left(\frac{\partial_X V}{V}\right)^2, \quad \eta_V = m_{\rm Pl}^2\left(\frac{\partial_X^2 V}{V}\right). \tag{2.2}$$

Here, $m_{\rm Pl} \simeq 2.43 \times 10^{18}$ GeV is the reduced Planck mass and $\partial_X \equiv \partial/\partial X$ with $X = \{\phi, \psi\}$ is the field derivative. In the slow roll limit, the spectral index n_s is given by [24],

$$n_s = 1 - 6\,\epsilon_V + 2\,\eta_V. \tag{2.3}$$

The central measurements by Planck 2018 in the ΛCDM model are; $n_s = 0.9647 \pm 0.012$ and the tensor to scalar ratio $r = 16\,\epsilon_V < 0.035$ at 95% C.L [25]. All the values are measured at the pivot scale, $k_0 = 0.05\,{\rm Mpc}^{-1}$. The subscript 0 from here and onward indicates the value at the pivot scale. Along the valley, one obtains the slow roll parameters eq. (2.2) to be,

$$\epsilon_V|_{\phi=\phi_c} \simeq \frac{m_{\rm Pl}^2}{2\,m_1^2} \quad \text{and} \quad \eta_V|_{\phi=\phi_c} \simeq -\frac{2\,m_{\rm Pl}^2}{m_2^2}. \tag{2.4}$$

The amplitude of the scalar power spectrum along the valley is given by,

$$A_s(k_0) = \left.\frac{V}{24\,\pi^2 m_{\rm Pl}^4\,\epsilon_V}\right|_{\phi=\phi_0}. \tag{2.5}$$

This amplitude is fixed by Planck's result $A_s(k_0) = 2.198 \times 10^{-9}$. Considering the vacuum energy to be the dominant source at the pivot scale, substituting the ϵ_V from eq. (2.4) and the amplitude of the scalar power spectrum in eq. (2.5), we obtained the relation between Λ and m_1,

$$\Lambda \simeq 2.198 \times 10^{-9} \times 12\,\pi^2\left(\frac{m_{\rm Pl}^6}{m_1^2}\right). \tag{2.6}$$

In our region of interest $m_1 \gg m_2$, following eq. (2.3), the scalar spectral index is now written as

$$n_s \simeq 1 - \frac{4\, m_{\rm Pl}^2}{m_2^2}. \tag{2.7}$$

The value of n_s in the ΛCDM model is $n_s = 0.9665 \pm 0.0038$ [26] that fixes $m_2 \simeq 11\, m_{\rm Pl}$. The corresponding value of n_s is shown in fig. 2 for the benchmark point (BP) in table 1 along with present and future plan experiments. The relevant number of e-folds, N_0, before the end of inflation are,

$$N_0 \simeq \left(\frac{1}{m_{\rm Pl}}\right)^2 \int_{X_e}^{X_0} \left(\frac{V}{V_X}\right) dX, \tag{2.8}$$

where X_e is the field value at the end of inflation which is fixed by the breakdown of the slow-roll approximation. The parameter set for different model variables we consider here is given in table 1.

Table 1: *Benchmark points for model parameters eq. (2.1)*

Model	$M/m_{\rm Pl}$	$\phi_c/m_{\rm Pl}$	$m_1/m_{\rm Pl}$	$m_2/m_{\rm Pl}$	$b/m_{\rm Pl}$	ϕ_i	ψ_i	N_k	r
BP	0.1	0.1	3.00×10^5	11	-8.00×10^9	$\phi_c(1{+}0.0011)$	ψ_0	55	2.89×10^{-11}

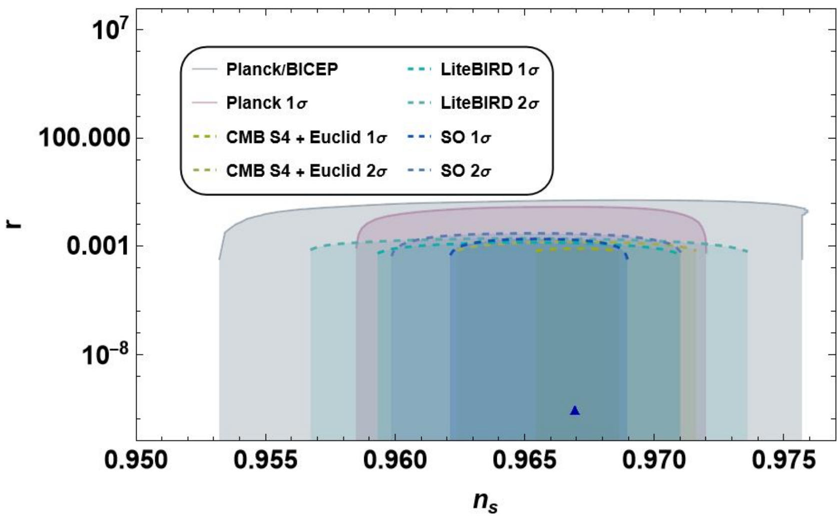

FIGURE 2: *Tensor-to-scalar ratio r vs. scalar spectral index n_s for the corresponding parameter sets given in table 1. The solid contours are the current Planck bounds [26], Planck/BICEP [25, 27, 28] and the dashed shaded region indicates the future proposed experiments (LiteBIRD, CMB-Euclid, Simons Observatory (SO)) [29–31].*

3 Numerical Treatment of Scalar Perturbations

The Klien-Gordon classical background equations of motion in the number of e-fold times are given by [32],

$$\phi'' + \left(\frac{H'}{H} + 3\right)\phi' + \frac{V_\phi}{H^2} = 0, \qquad \psi'' + \left(\frac{H'}{H} + 3\right)\psi' + \frac{V_\psi}{H^2} = 0. \tag{3.1}$$

Here, $V_X = dV/dX$ where, $X = \{\phi, \psi\}$, prime is the derivative with respect to the number of e-folds and the Hubble rate H is defined as $H^2 = 2\,V/(6 - \phi'^2 - \psi'^2)$. The evolution of the field from pivot scale till the end of inflation, $\epsilon_V = 1$, is shown in fig. 9. The scalar perturbations of the FLRW metric in longitudinal gauge can be expressed as [32],

$$ds^2 = a^2\left[(1+2\,\Phi_{\rm B})d\tau^2 + \left[(1-2\,\Psi_{\rm B})\delta_{ij} + \frac{h_{ij}}{2}\right]dx^i dx^j\right], \tag{3.2}$$

where τ is the conformal time related to cosmic time via scale factor a, $dt = a\,d\tau$, $\Phi_{\rm B}$ and $\Psi_{\rm B}$ are the Bardeen potentials and h_{ij} is the transverse-traceless tensor metric perturbation. We work in a conformal Newtonian gauge such that $\Phi_{\rm B} = \Psi_{\rm B}$. The scalar perturbations are defined as [32, 33],

$$\delta X_i^{''} + (3-\epsilon)\delta X_i^{'} + \sum_{j=1}^{2}\frac{1}{H^2}V_{X_iX_j}\delta X_j + \frac{k^2}{a^2H^2}\delta X_i = 4\Phi_{\rm B}^{'}X_i^{'} - \frac{2\,\Phi_{\rm B}}{H^2}V_{X_i}. \tag{3.3}$$

Here X with the subscript (i,j) refers to the fields $(\phi,\,\psi)$, k is the comoving wave number, the equation of motion for $\Phi_{\rm B}$ is given by,

$$\Phi_{\rm B}^{''} + (7-\epsilon)\Phi_{\rm B}^{'} + \left(\frac{2V}{H^2} + \frac{k^2}{a^2H^2}\right)\Phi_{\rm B} + \frac{V_{X_i}}{H^2}\delta X_i = 0. \tag{3.4}$$

The initial conditions (i.c) for field perturbations in e-fold time are given as,

$$\delta X_{i,\rm i.c} = \frac{1}{a_{\rm i.c}\sqrt{2k}}, \qquad \delta X_{i,\rm i.c}^{'} = -\frac{1}{a_{\rm i.c}\sqrt{2k}}\left(1 + \iota\frac{k}{a_{\rm i.c}H_{\rm i.c}}\right). \tag{3.5}$$

The initial conditions for the Bardeen potential and its derivative are given by,

$$\Phi_{\rm B,i.c} = \sum_{j=1}^{2}\frac{\left(H_{\rm i.c}^2X_{i,\rm i.c}^{'}\delta X_{i,\rm i.c}^{'} + \left(3H_{\rm i.c}^2X_{i,i.c}^{'} + V_{X_i,\rm i.c}\right)\delta X_{i,\rm i.c}\right)}{2H_{\rm i.c}^2\left(\epsilon_{\rm i.c} - \frac{k^2}{a_{\rm i.c}^2H_{\rm i.c}^2}\right)}, \tag{3.6}$$

$$\Phi_{\rm B,i.c}^{'} = -\Phi_{\rm B,i.c} + \sum_{j=1}^{2}\frac{X_{i,\rm i.c}^{'}\delta X_{i,\rm i.c}}{2}.$$

The scalar power spectrum in terms of curvature perturbations ζ is given by,

$$P_R(k) = \frac{k^3}{2\pi^2}\left|\zeta\right|^2 = \frac{k^3}{2\pi^2}\left|\Phi_{\rm B} + \frac{\sum_{i=1}^{2}X_i^{'}\delta X_i}{\sum_{j=1}^{2}X_j^{'2}}\right|^2. \tag{3.7}$$

We, later on, use this relation to numerically evaluate the power spectrum.

4 Power Spectrum Analytical Expression

In this section, we provide an analytical expression for the scalar power spectrum following Ref. [19]. To calculate the analytical expression for the power spectrum, let us begin with the slow roll approximation (in units $m_{\rm Pl} = 1$) under which the Klein-Gordon equations with respect to the number of e-folds can be written as,

$$3\,H^2\phi^{'} = -V_\phi = -\Lambda\left(\frac{1}{m_1} + \frac{8\,\phi^3\psi^2}{M^2\,\phi_c^4}\right), \tag{4.1}$$

$$3\,H^2\psi^{'} = -V_\psi = -\Lambda\left(b^{-1} + \frac{4\,\phi^4\psi}{M^2\,\phi_c^4} - \frac{4\,\psi}{M^2}\left(1 - \frac{\psi^2}{M^2}\right)\right).$$

There are three different phases in the waterfall regime and only phase-1 is important [19] during which, the above equations reduce to,

$$
\begin{aligned}
3\,H^2\phi^{'} &= -\Lambda\left(\frac{1}{m_1}\right), \\
3\,H^2\psi^{'} &= -\Lambda\left(b^{-1} + \frac{4\,\phi^4\psi}{M^2\,\phi_c^4} - \frac{4\,\psi}{M^2}\right).
\end{aligned}
\tag{4.2}
$$

Defining $H^2 = \Lambda/3$, eq. (4.2) becomes,

$$
\begin{aligned}
\phi^{'} &= -\left(\frac{1}{m_1}\right), \\
\psi^{'} &= -\left(b^{-1} + \frac{4\,\phi^4\psi}{M^2\,\phi_c^4} - \frac{4\,\psi}{M^2}\right).
\end{aligned}
\tag{4.3}
$$

Let us assume the solution,

$$
\phi = \phi_c\, e^{\xi}, \qquad \psi = \psi_0\, e^{\chi}. \tag{4.4}
$$

Under the slow roll approximation, during the waterfall, $|\xi| \ll 1$, one can write;

$$
\phi \simeq \phi_c\,(1+\xi)\,, \qquad \psi = \psi_0\, e^{\chi}. \tag{4.5}
$$

Here, ψ_0 is the auxiliary field distribution width at the critical point of instability given by [10],

$$
\psi_0 = \sqrt{\frac{\Lambda\, M\,\sqrt{2\,\phi_c\, m_1}}{92\,\pi^{3/2}\, m_{\rm Pl}^4}}. \tag{4.6}
$$

Under solutions eq. (4.5) and taking into account $|\xi| \ll 1$, one can write eq. (4.3) as,

$$
\begin{aligned}
\xi^{'} &\simeq -\left(\frac{1}{m_1\,\phi_c}\right), \\
\chi^{'} &= -\left(\frac{b^{-1}}{\psi_0\, e^{\chi}} + \frac{4\,\phi_c^4}{M^2\,\phi_c^4}\,(1+\xi)^4 - \frac{4}{M^2}\right) \\
&\simeq -\left(\frac{b^{-1}}{\psi_0\, e^{\chi}} + \frac{4\,\phi_c^4}{M^2\,\phi_c^4}\,(1+4\,\xi) - \frac{4}{M^2}\right).
\end{aligned}
\tag{4.7}
$$

This gives,

$$
\frac{d\xi}{d\chi} = \frac{1}{m_1\,\phi_c\left(\frac{b^{-1}}{\psi_0\, e^{\chi}} + \frac{4\,\phi_c^4}{M^2\,\phi_c^4}\,(1+4\,\xi) - \frac{4}{M^2}\right)}. \tag{4.8}
$$

Solving eq. (4.7) for ξ_N one gets,

$$
\xi \simeq -\frac{1}{m_1\,\phi_c}\,N. \tag{4.9}
$$

Or one can write,

$$
N \simeq -m_1\,\phi_c\,\xi. \tag{4.10}
$$

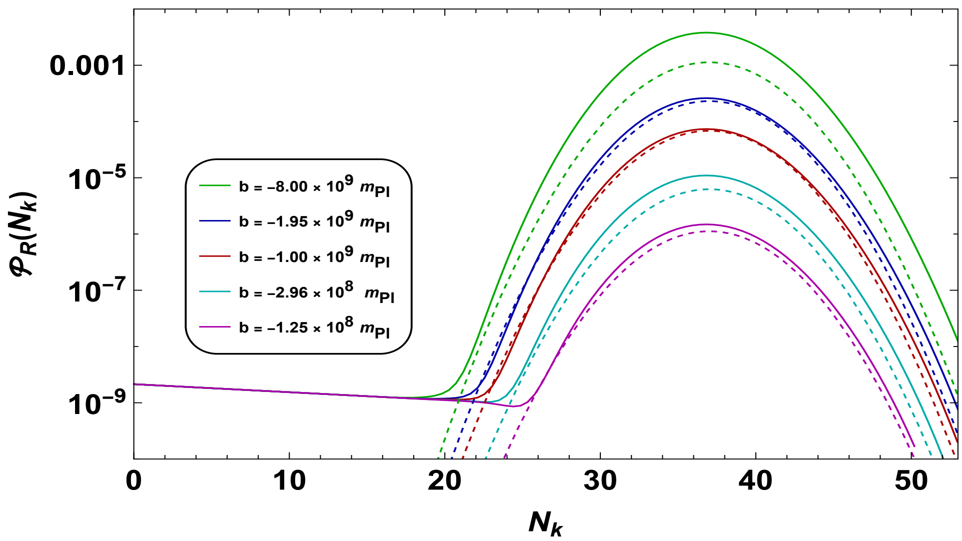

FIGURE 3: *Power spectrum by solving the exact linear scalar perturbation equations (solid) eq. (3.7) and for the analytical expression (dashed) eq. (4.19) for the BP in table 1.*

The above equation gives the number of e-folds in phase-1. Consider eq. (4.8), it is not easy to solve analytically. Let us consider the approximation $\psi_0\, e^{\chi} \simeq \psi_0$, assuming $\chi \ll \xi$,

$$\frac{d\xi}{d\chi} \simeq \frac{1}{m_1\,\phi_c \left(\dfrac{b^{-1}}{\psi_0} + \dfrac{4}{M^2}\,(4\,\xi)\right)}. \tag{4.11}$$

This implies,

$$\xi \simeq \frac{-b^{-1}\,M^4\,m_1 + M^2\sqrt{m_1\,\left(b^{-2}\,M^4\,m_1 + 32\,\phi_c\,\psi_0^2\,\chi\right)}}{16\,\psi_0\,m_1\phi_c^2}. \tag{4.12}$$

Therefore, the number of e-folds in phase-1 are,

$$N_1 \simeq -\xi\,m_1\,\phi_c \simeq \frac{-b^{-1}\,M^4\,m_1 + M^2\sqrt{m_1\,\left(b^{-2}\,M^4\,m_1 + 32\,\phi_c\,\psi_0^2\,\chi\right)}}{16\,\psi_0\,\phi_c}. \tag{4.13}$$

Using the δ-N formalism, the scalar power spectrum is given by,

$$P_R = \frac{H^2}{4\,\pi^2}\left(N_{,\psi}^2 + N_{,\phi}^2\right). \tag{4.14}$$

Here, $N_{,\xi} = dN/d\xi$, $N_{,\psi} = N_{1,\psi}$ and $N_{,\phi} = N_{1,\phi}$ since the dominant contribution comes from phase-1 [32]. Taking the derivative with respect to ψ of eq. (4.13) gives

$$N_{1,\psi} = \frac{-M^2\,\sqrt{m_1}\psi_0}{\psi_k\sqrt{b^{-2}\,M^4\,m_1 + 32\,\phi_c\,\psi_0^2\,\chi_2}}. \tag{4.15}$$

Here, $\psi_k \equiv d\psi/d\chi = \psi_0\,e^{\chi_k}$. One can calculate χ_k by solving eq. (4.11) and eq. (4.9),

$$\chi_k = \frac{8\,\left(N_k - N_{\rm e}\right)^2}{M^2\,m_1\,\phi_c} - b_1^{-1}\,\left(N_k - N_{\rm e}\right), \tag{4.16}$$

where, N_k, $N_{\rm e}$ are the number of e-folds at the pivot scale, at the end of inflation respectively and we absorb the constant by redefining $b_1^{-1} \longrightarrow b^{-1}/\psi_0$. This reduces eq. (4.15) to,

$$N_{1,\psi} = \frac{-M^2\sqrt{m_1}}{\sqrt{b^{-2}\,M^4\,m_1 + 32\,\phi_c\,\psi_0^2\,\chi_2}}\,\frac{1}{\exp\left(\dfrac{8\,(N_k - N_{\rm e})^2}{M^2\,m_1\,\phi_c} - b_1^{-1}\,(N_k - N_{\rm e})\right)}. \tag{4.17}$$

Similarly, from eq. (4.9) one can write $N_{1,\phi}$ as,

$$N_{1,\phi} \simeq m_1\,\phi_c\,\frac{d\xi}{d\phi} \simeq -m_1. \tag{4.18}$$

The power spectrum eq. (4.14) now becomes,

$$P_R \simeq \frac{H^2}{4\,\pi^2}\left(\frac{m_1^2}{m_{\rm Pl}^4} + \left(\frac{\digamma\,M^2\sqrt{m_1}\,e^{-\left(\dfrac{8\,m_{\rm Pl}^4\,(N_k - N_{\rm e})^2}{M^2\,m_1\,\phi_c} - b^{-1}\,m_{\rm Pl}\,(N_k - N_{\rm e})\right)}}{m_{\rm Pl}^3\sqrt{b^{-2}\,M^4\,m_1 + 32\,\phi_c\,\psi_0^2\,\chi_2}}\right)^2\right). \tag{4.19}$$

Here, we introduce a fudge factor $\digamma = 10^{-1}$ to keep the consistency of the previously used approximations and recover the Planckian units. In fig. 3, we present an exact power spectrum (numerically solved) along with the analytical expression given in eq. (4.19) for the potential eq. (2.1) and the BP in table 1. This clearly represents that the linear term helps to reduce the height of the power spectrum. The analytical expression is slightly off for the larger values of b since estimations were made to obtain eq. (4.17). It is important to note that the analytical expression overestimates the power spectrum due to the fact that if we do not implement the assumption in eq. (4.11), the parameter b^{-1} will evolve as a decreasing function due to the increasing behavior of the waterfall field. Therefore, the exponential factor would be suppressed. The width of the power spectrum is defined by the number of e-folds in the waterfall regime and hence is not affected by the underlying assumption.

5 Embedding in a Realistic Framework: Sneutrino Hybrid Inflation

In this section, we explore the SUSY imprints in the SIGWs and the PBHs. We explore the supersymmetric hybrid inflation as a realistic model where the inflation is driven by a singlet sneutrino $\tilde{N}_R$. Consider the superpotential [34],

$$W = \kappa S\left(\frac{\hat{\phi}^4}{M'^2} - M_1^2\right) + \frac{(\lambda_N)}{M_\star}\,\hat{N}\hat{N}\,\hat{\phi}\hat{\phi} + \dots\,, \tag{5.1}$$

where κ and (λ_N) are dimensionless Yukawa couplings and M', M_1 and $M_\star$ are three independent mass parameters. The superfields $\hat{N}$, $\hat{\phi}$ and $\hat{S}$ contain the bosonic components which are respectively: the singlet sneutrino $\hat{N}$ which plays the role of the inflaton; the waterfall field $\hat{\phi}$, which is not exactly at zero during inflation but slightly off due to the presence of the linear term and develops a non-zero vacuum expectation value (vev) after inflation; and the singlet field S which is held at zero during and after inflation. Note that we assume a Z_4 symmetry to prevent an explicit right-handed (s)neutrino mass for the superfield containing the inflaton. Any other RH neutrinos are assumed to be singlets under the Z_4 and have large explicit masses.

The vev of the waterfall field after inflation is fixed by the first term on the right-hand side in eq. (5.1). During inflation, this term contributes a large vacuum energy to the potential. The waterfall superfield appears as $\hat{\phi}^4/M'^2$ which will prevent the explicit singlet sneutrino masses via Z_4 discrete symmetry but this will be softly broken due to the presence of the linear term. The superpotential eq. (5.1) also respect the $U(1)_R$-symmetry and carries unit R-charge by assigning unit to $\hat{S}$ and 1/2 to $\hat{N}$ The discrete subgroup of Z_4 symmetry acts as a matter parity under suitable conditions [35, 36]. The Kähler potential with non-zero F-terms during inflation is given as [34]

$$\begin{aligned} \mathrm{K} = |\hat{S}|^2 + |\hat{\phi}|^2 + |\hat{N}|^2 + \kappa_S \frac{|\hat{S}|^4}{4\, m_{\mathrm{Pl}}^2} + \kappa_N \frac{|\hat{N}|^4}{4\, m_{\mathrm{Pl}}^2} + \kappa_\phi \frac{|\hat{\phi}|^4}{4\, m_{\mathrm{Pl}}^2} + \kappa_{S\phi} \frac{|\hat{S}|^2 |\hat{\phi}|^2}{m_{\mathrm{Pl}}^2} \\ + \kappa_{SN} \frac{|\hat{S}|^2 |\hat{N}|^2}{m_{\mathrm{Pl}}^2} + \kappa_{N\phi} \frac{|\hat{N}|^2 |\hat{\phi}|^2}{m_{\mathrm{Pl}}^2} + \dots \end{aligned} \tag{5.2}$$

where the dots are for higher-order terms and $m_{\mathrm{Pl}} = 2.43 \times 10^{18}$ GeV is the reduced Planck mass. The field S acquires a large mass and sits at zero during inflation. The F-term scalar potential is given by [34],

$$V_F = e^{\mathrm{K}/m_{\mathrm{Pl}}^2} \left(K_{ij}^{-1} D_{z_i} \mathrm{W} D_{z_j^*} \mathrm{W}^* - 3 \frac{|\mathrm{W}|^2}{m_{\mathrm{Pl}}^2} \right). \tag{5.3}$$

Here, $z_i \in \{\hat{N}, \hat{\phi}, \hat{S} \dots\}$ are the bosonic components of the superfields and,

$$D_{zi} = \frac{\partial \mathrm{W}}{\partial z_i} + \frac{\mathrm{W}}{m_{\mathrm{Pl}}^2} \frac{\partial \mathrm{K}}{\partial z_i}, \quad K_{ij} = \frac{\partial^2 \mathrm{K}}{\partial z_i \partial z_j^*}, \quad \text{and} \quad D_{z_j^*} \mathrm{W}^* = (D_{z_j} \mathrm{W})^*. \tag{5.4}$$

Assuming that $\tilde{N}, \tilde{\phi}$ and S are effective gauge singlets and there are no relevant D-terms at the considered energy scale. In terms of real fields, the scalar potential for sneutrino hybrid inflation close to the critical point of instability, using eqs. (5.1) and (5.2). We also incorporate a soft-breaking of Z_4-symmetry with a linear term, which as we will show will inflate topological defects and help us to control PBH overproduction [13, 37] can be written as [34],

$$\begin{aligned} V(\tilde{N}_R, \tilde{\phi}) \supseteq \kappa^2 M_1^4 \Bigg(1 - \frac{\beta}{2} \left(\frac{\tilde{\phi}}{m_{\mathrm{Pl}}} \right)^2 - \left(\frac{1}{M_1 M'} \right)^2 \tilde{\phi}^4 + \frac{\gamma}{2\, m_{\mathrm{Pl}}^2} \left(\tilde{N}_R - \tilde{N}_{Rc} \right)^2 \\ + c_1^3 \left(\frac{\tilde{N}_R - \tilde{N}_{Rc}}{\kappa^2 M_1^4} \right) + \frac{\lambda_N^2}{2\, M_\star^2\, \kappa^2\, M_1^4} \tilde{N}_R^4 \tilde{\phi}^2 + b_1^3 \frac{\tilde{\phi}}{\kappa^2 M_1^4} \Bigg). \end{aligned} \tag{5.5}$$

Here, β and γ are dimensionless couplings defined as [34],

$$\beta = \kappa_{S\phi} - 1, \qquad \gamma = 1 - \kappa_{SN}. \tag{5.6}$$

The coefficients of the linear terms c_1 and b_1 are dimensionful parameters and b_1 controls the peak of the scalar power spectrum to avoid PBH overproduction, as discussed in sections 2 and 4. The schematic view of the hybrid potential is shown in fig. 1.

5.1 Comparing Model Parameters and Power Spectrum

Let us now fix the BPs for eq. (5.5) by comparing with the toy model eq. (2.1), we identify,

$$\begin{aligned} \kappa^2 M_1^4 = \Lambda, \qquad M_1^2 M'^2 = M^4, \qquad \frac{\beta}{2\, m_{\mathrm{Pl}}^2} = \frac{2}{M^2}, \qquad \frac{-\gamma}{2\, m_{\mathrm{Pl}}^2} = \frac{1}{m_2^2} \\ \frac{\lambda_N^2}{2\, M_\star^2\, \kappa^2\, M_1^4} = \frac{1}{M^2\, \phi_c^4}, \qquad \frac{b_1^3}{\kappa^2 M_1^4} = \frac{1}{b}, \qquad \frac{c_1^3}{\kappa^2 M_1^4} = \frac{1}{m_1}. \end{aligned} \tag{5.7}$$

Following eq. (4.6), the auxiliary field distribution width can be written as,

$$\phi_0 = \left(\frac{\kappa^2 M_1^4}{92\,\pi^{3/2}\, m_{\rm Pl}^4} \sqrt{\frac{2\, M_1\, M'\, \tilde{N}_{Rc}}{c_1^3}} \right)^{1/2} . \tag{5.8}$$

The benchmark point for the potential eq. (5.5) is given in table 2. The abundance of PBH for the benchmark point in table 2 is shown in fig. 6 that explains the PBHs as DM entirely or some fraction of it. The model predicts the scalar spectral index, n_s and the tensor to scalar ratio, r consistent with recent Planck 2018 results [26]. Following eqs. (2.4) and (2.7) we obtain,

$$n_s \simeq 1 + 2\,\gamma, \qquad r = 16\,\epsilon_V \simeq \frac{m_{\rm Pl}^2\, c_1^6}{2\,\Lambda^2}. \tag{5.9}$$

This fixes $\gamma = -0.017$ for the central value of n_s. The mass squared of the waterfall field at $\tilde{\phi} = 0$ is

$$M_{\tilde{\phi}}^2 = \left(-\frac{\kappa^2\, M_1^4\, \beta}{m_{\rm Pl}^2} + \frac{\lambda_N^2}{M_\star^2} \tilde{N}_R^4 \right). \tag{5.10}$$

In this paper, we assume that $(\lambda_N/M_\star)^2 > \kappa^2\,\beta/(m_{\rm Pl}^2)$ such that $M_{\tilde{\phi}}^2 > 0$ at large $\tilde{N}_R > \tilde{N}_{Rc}$ to stabilize the inflationary trajectory at $\tilde{\phi} = 0$, where,

$$\tilde{N}_{Rc} = \left(\frac{\kappa^2\, M_1^4\, M_\star^2\, \beta}{m_{\rm Pl}^2\, \lambda_N^2} \right)^{1/4} . \tag{5.11}$$

During inflation, as long as $\tilde{N}_R \lesssim \tilde{N}_{Rc}$, the effective mass square of $\tilde{\phi}$ becomes negative, giving rise to tachyonic instability that will grow the curvature perturbations. These growing perturbations will enhance the scalar power spectrum at small scales and upon horizon re-entry the collapse of large density fluctuations produces the PBHs. When the waterfall field acquires a non-zero vev during the waterfall transition, the positive mass square term yields the masses of the singlet sneutrinos. The benchmark points are given in table 2 for the potential in eq. (5.5) for the production of PBH and induced SGWB.

The field evolution from the pivot scale to the end of inflation is given in fig. 4 for the BPs in table 2. The exact power spectrum eq. (3.7) is given in fig. 5 from the pivot scale till the end of inflation. The power spectrum is constrained by the angular resolution of current CMB measurements at scales $10^{-4} \lesssim k/\text{Mpc}^{-1} \lesssim 1$. However, inhomogeneities at these scales result in isotropic deviations from the usual blackbody spectrum and are known as spectral distortions [38]. There are two major categories of these distortions: μ-distortions, associated

Table 2: *Benchmark points for model–1 parameters*

Model	$M_1/m_{\rm Pl}$	$M_\star/m_{\rm Pl}$	$-(M'/m_{\rm Pl})^2$	β	λ_N	κ	$b_1/m_{\rm Pl}$	$c_1/m_{\rm Pl}$
BP-1	1.00×10^{-2}	1.0	-1.0	384.5	1.73×10^{-6}	8.50×10^{-6}	-9.11×10^{-11}	1.4×10^{-8}
BP-2	9.02×10^{-3}	1.0	-1.0	443.2	2.14×10^{-6}	1.13×10^{-5}	-9.11×10^{-11}	1.4×10^{-8}
BP-3	8.10×10^{-3}	1.0	-1.0	493.8	2.52×10^{-6}	1.40×10^{-5}	-9.11×10^{-11}	1.4×10^{-8}

Model	γ	$\tilde{N}_{Rc}/m_{\rm Pl}$	$\tilde{N}_{Ri}/m_{\rm Pl}$	$\tilde{\phi}_i/m_{\rm Pl}$	N_k	n_s	r	T_R/**GeV**
BP-1	-0.017	0.100	$\tilde{N}_{Rc}(1{+}0.001)$	ϕ_0	58	0.966	2.89×10^{-11}	5.6×10^7
BP-2	-0.017	0.095	$\tilde{N}_{Rc}(1{+}0.001)$	ϕ_0	53	0.966	3.25×10^{-11}	6.3×10^7
BP-3	-0.017	0.090	$\tilde{N}_{Rc}(1{+}0.001)$	ϕ_0	48	0.966	3.62×10^{-11}	6.8×10^7

with chemical potential that occurs at early times, and Compton y-distortions, generated at redshifts $z \lesssim 5\times10^4$. A μ-distortion is associated with a Bose-Einstein distribution with

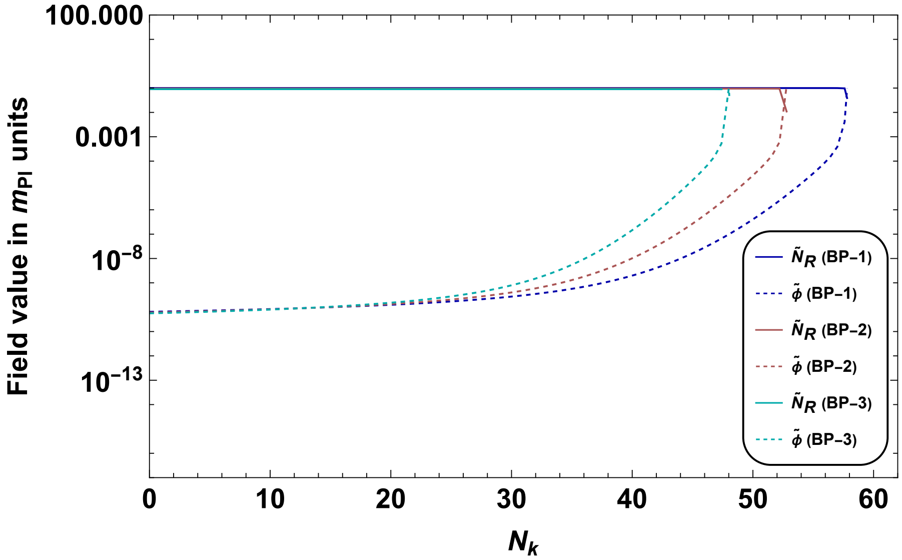

FIGURE 4: *Fields evolution with the number of e-folds from pivot scale to the end of inflation. We evaluate solving the full background eq. (3.1) using the potential given in eq. (5.5) for the benchmark points in table 2.*

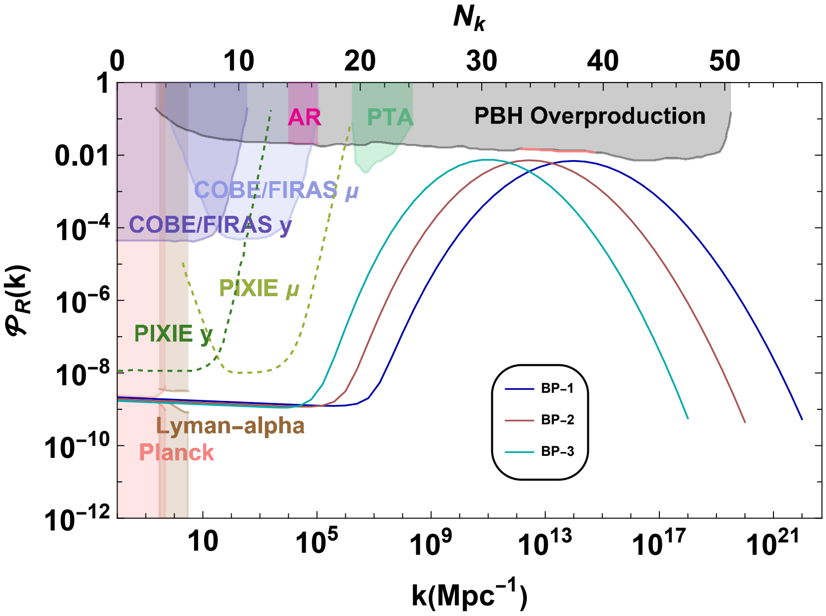

FIGURE 5: *Power spectrum by solving the exact linear scalar perturbation equations eq. (3.7) with the shaded region corresponding to the constraints from the present (solid) and future (dashed) experiments. The corresponding set of parameters are given in table 2.*

$\mu \neq 0$. Currently, the COBE/FIRAS instruments put the most stringent constraints on spectral distortions, which restricts $|\mu| \lesssim 9.0 \times 10^{-5}$ and $|y| \lesssim 1.5 \times 10^{-5}$ at the 95% C.L [39]. A PIXIE-like detector can investigate distortions with magnitudes $\mu \lesssim 2 \times 10^{-8}$ and $y \lesssim 4 \times 10^{-9}$ [40]. We find that our model parameters in table 2 satisfy the constraints of COBE/FIRAS. It is important to note that in the BPs table 2, although the mass scale M is sub-Planckian the coupling β is such a large number. We will see later in section 8 that it can be controlled by introducing a field transformation by the so-called α-attractor.

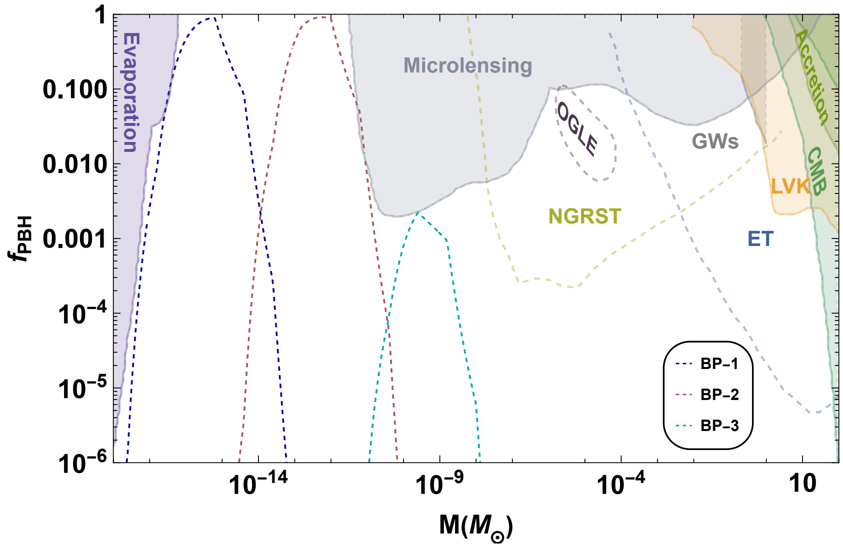

FIGURE 6: *PBH abundance as DM given in eq. (6.2). The shaded regions represent the observational constraints on the PBH abundance from various experiments, see the main text for the details.*

6 PBH abundance

The mass of PBH formation is associated with a wave vector k and is given by [41],

$$M_{\rm PBH} = 3.68 \left(\frac{\gamma_c}{0.2}\right) \left(\frac{g_*(T_f)}{106.75}\right)^{-1/6} \left(\frac{10^6\,{\rm Mpc}^{-1}}{k}\right)^2 M_{\odot}. \tag{6.1}$$

The fractional abundance of PBHs, $\Omega_{\rm PBH}/\Omega_{\rm DM} \equiv f_{\rm PBH}$ is defined as [41],

$$f_{\rm PBH} = \frac{\beta(M_{\rm PBH})}{3.94\times 10^{-9}} \left(\frac{g_*(T_f)}{106.75}\right)^{-1/4} \left(\frac{\gamma_c}{0.2}\right)^{1/2} \left(\frac{0.12}{\Omega_{\rm DM} h^2}\right) \left(\frac{M_{\rm PBH}}{M_{\odot}}\right)^{-1/2}, \tag{6.2}$$

where $M_{\rm PBH}$ is the PBH mass, the current energy density of DM is $h^2\Omega_{\rm DM} = 0.12$, $\gamma_c = 0.2$ is the factor depends on the gravitational collapse and β is the fractional energy density at the time of formation and is given by [42],

$$\beta(M_{\rm PBH}) = \frac{1}{2\pi\sigma^2(M_{\rm PBH})} \int_{\delta_c}^{\infty} d\delta\, \exp\left(-\frac{\delta^2}{2\sigma^2\,(M_{\rm PBH})}\right). \tag{6.3}$$

The variance, $\sigma(M_{\rm PBH})$ of curvature perturbations ranges between $\sigma^2(M_{\rm PBH}) \simeq 10^{-2} - 10^{-3}$ which corresponds to the critical threshold, $\delta_c \simeq 0.4-0.6$ [43–46] to explain the entire abundance of DM. Mathematically, the variance is defined as [42],

$$\sigma^2(M_{\rm PBH}(k)) = \frac{16}{81} \int \frac{dk'}{k'} (k'/k)^4 W^2(k'/k) P_s(k'), \tag{6.4}$$

where $W(x) = \exp(-x^2/2)$ is the Gaussian window function and $P_s(k)$ is the scalar power spectrum defined in eq. (3.7).

In fig. 6, the PBH abundance eq. (6.2) is demonstrated along with the different experimental constraints [47] for given parameter sets in table 2. For BP-1, the entire abundance of DM can be explained by PBH. The Hawking radiations may evaporate the PBHs and therefore there are some constraints in microlensing-related observations such as: CMB [48], EDGES [49], INTEGRAL [50, 51], Voyager [52], 511 keV [53], EGRB [54]; HSC (Hyper-Supreme Cam) [55], EROS [56], OGLE [57] and Icarus [58]; if PBHs accrete, there are constraints due to the CMB spectrum ref. [59]; finally the range around $M_\odot$ is constrained by LIGO-VIRGO-KAGRA observations on PBH-PBH merger [60–62]). Future planned GW interferometers like Einstein Telescope (ET) and Cosmic Explorer (CE) are also expected to set limits on the PBH abundance see refs. [63, 64], these are shown in dashed lines in the plot. Future sensitivity reaches of the Nancy Roman Telescope from micro-lensing are also presented, see ref. [65].

7 Scalar-induced GWs

We assume that the formation of PBH in the radiation-dominated era, the energy density of GWs today in terms of scalar power spectrum eq. (3.7), is given by [66, 67],

$$\Omega_{\rm GW}(k) = \frac{c_g\,\Omega_r}{6}\left(\frac{g_*(T_f)}{106.75}\right)\int_{-1}^{1} dd \int_{1}^{\infty} ds\; P_s\left(k\frac{s-d}{2}\right) P_s\left(k\frac{s+d}{2}\right) I(d,s), \tag{7.1}$$

$$I(d,s) = \frac{288(d^2-1)^2(s^2-1)^2(s^2+d^2-6)^2}{(d-s)^8(d+s)^8}\left\{\left(d^2-s^2+\frac{d^2+s^2-6}{2}\ln\left|\frac{s^2-3}{d^2-3}\right|\right)^2 \right.$$
$$\left. \frac{\pi^2}{4}(d^2+s^2-6)^2\Theta(s-\sqrt{3})\right)\Bigg\}.$$

Here, $\Omega_r = 5.4\times10^{-5}$ is the present-day energy density of the radiation, $c_g = 0.4$ in the SM, Θ is the Heaviside function, and $g_*(T_f) \simeq 106.75$ is the effective degrees of freedom at the temperature T_f of PBH formation for SM like spectrum. Furthermore, using $k = 2\pi f$, $1\text{Mpc}^{-1} = 0.97154\times10^{-14}\,\text{s}^{-1}$ and $h = 0.68$, we move into the $h^2\Omega_{\rm GW}(f) - f$ plane. The GW spectra for the benchmark points in table 2 are shown in fig. 7 with the different experiments presented by the shaded region such as, SKA [68], THEIA [69], LISA [70], μ-ARES [71], BBO [72], U-DECIGO [73, 74], CE [75] and ET [76].

Searching for stochastic GW of cosmic origin is likely to reveal multiple astrophysical sources of GW background. They can primarily take the form of binary neutron star (NS-NS) events [79] and LIGO/VIRGO detected binary black hole (BH-BH) merging events [77, 78]. To differentiate with the scalar-induced GWs of cosmic origin, the foreground NS and BH can be subtracted using the sensitivities of the BBO and ET / CE windows, especially in the range $\Omega_{\rm GW} \simeq 10^{-15}$ [80] and $\Omega_{\rm GW} \simeq 10^{-13}$ [81]. The binary white dwarf galactic and extra-galactic (WD-WD) can be removed [83] with the expected sensitivity at $\Omega_{\rm GW} \simeq 10^{-13}$ [84], and may be more significant than the NS-NS and BH-BH foregrounds in the LISA window [82]. The GW spectrum generated by the astrophysical foreground grew with frequency $\propto f^{2/3}$ in addition to this subtraction [85]. This GW spectrum differs from that produced by second-order gravitational waves, which at low frequencies convict as $f^{3/2}$ and at higher frequencies as $f^{-3/2}$. This will allow us to identify the GW signals generated by scalar-induced sources.

8 *Model*−2: α-attractor sneutrino hybrid inflation

In this section, we explore the supersymmetric hybrid inflation in the context of an exponential α-attractor model [89]. As we have mentioned the predictions for the coupling β is a very large number see table 2 in the previous sneutrino model. So, here we propose a variation of the sneutrino model where we will see that with the field redefinition in terms of α-attractor, this parameter takes a natural value. In terms of real fields, the scalar potential for sneutrino hybrid inflation (including a linear term) can be written as [34],

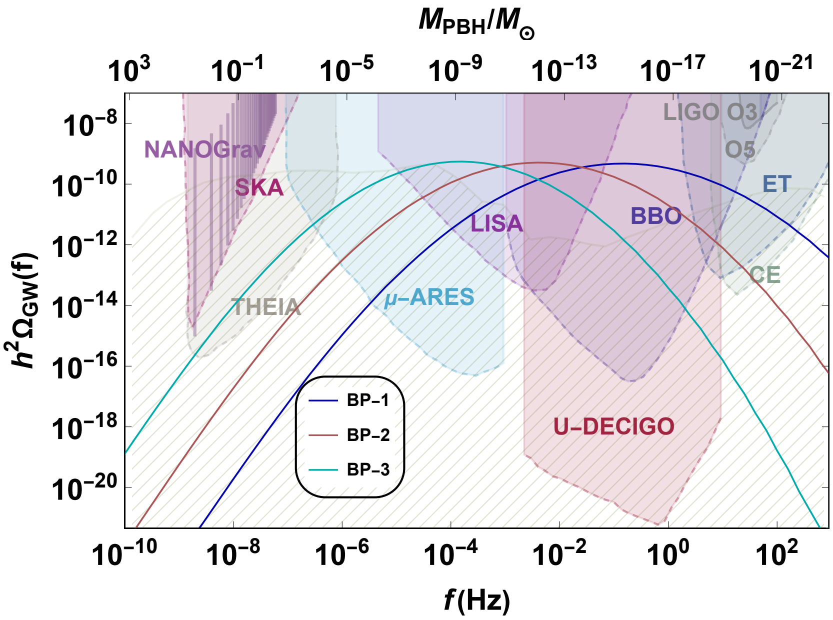

FIGURE 7: *The energy density of gravitational waves for eq. (7.1) for the BPs in table 2. The colored shaded regions indicate the sensitivity curves of present (solid boundaries) LIGO O3 [86], NANOGrav [87] and future (dashed boundaries) LIGO O5, SKA [68], THEIA [69], LISA [70], μ-ARES [71], BBO [72], U-DECIGO [73, 74], CE [75] and ET [76] experiments. The hatched region shows the astrophysical background [88].*

$$V(\tilde{N}_R,\tilde{\phi}) \supseteq \kappa^2 M^4 - \frac{\kappa^2 M^4 \beta}{2}\left(\frac{\tilde{\phi}}{m_{\rm Pl}}\right)^2 - \kappa^2\left(\frac{M}{M'}\right)^2\tilde{\phi}^4 + \frac{\kappa^2 M^4 \gamma}{2}\left(\frac{\tilde{N}_R}{m_{\rm Pl}}\right)^2 + \frac{\lambda_N^2}{2 M_\star^2}\tilde{N}_R^4\tilde{\phi}^2 + d^3\tilde{\phi} \tag{8.1}$$

with all the parameters as defined for eq. (5.5). The coefficient of the linear term d is a dimensionful parameter that will again allow us to control the peak of the scalar power spectrum to avoid PBH overproduction. The canonical transformation of the inflaton field $\tilde{N}_R \longrightarrow \sqrt{6\,\alpha}\,{\rm Tanh}\left(\tilde{\upsilon}_R/\sqrt{6\,\alpha}\right)$, allows us to write eq. (8.1) as,

$$V(\tilde{\upsilon}_R,\tilde{\phi}) = \kappa^2 M^4 - \frac{\kappa^2 M^4 \beta}{2}\left(\frac{\tilde{\phi}}{m_{\rm Pl}}\right)^2 - \kappa^2\left(\frac{M}{M'}\right)^2\tilde{\phi}^4 + \frac{\kappa^2 M^4 \gamma}{2}\left(\frac{\sqrt{6\,\alpha}\,{\rm Tanh}\left(\tilde{\upsilon}_R/\sqrt{6\,\alpha}\right)}{m_{\rm Pl}}\right)^2 + \frac{\lambda_N^2}{2 M_\star^2}\left(\sqrt{6\,\alpha}\,{\rm Tanh}\left(\frac{\tilde{\upsilon}_R}{\sqrt{6\,\alpha}}\right)\right)^4\tilde{\phi}^2 + d^3\tilde{\phi}. \tag{8.2}$$

The benchmark point for potential eq. (8.2) is given in table 3. The PBH abundance as DM for the benchmark point in table 3 is shown in fig. 11. The model predicts the scalar spectral index, n_s and the tensor to scalar ratio, r consistent with recent Planck 2018 results [26]. The squared mass of the waterfall field at $\tilde{\phi} = 0$ is,

$$M_{\tilde{\phi}}^2 = \left(-\frac{\kappa^2 M^4 \beta}{2 m_{\rm Pl}^2} + \frac{\lambda_N^2}{M_\star^2} \left(\sqrt{6}\,\alpha\, {\rm Tanh}\left(\frac{\tilde{\upsilon}_R}{\sqrt{6}\,\alpha} \right) \right)^4 \right). \tag{8.3}$$

Assuming $(\lambda_N\, 6\,\alpha/M_\star)^2 > \kappa^2 M^4 \beta/(2\, m_{\rm Pl}^2)$ such that $M_{\tilde{\phi}}^2 > 0$ at large $\tilde{\upsilon}_R > \tilde{\upsilon}_{Rc}$ to stabilize the inflationary trajectory at $\tilde{\phi} = 0$, where,

$${\rm Tanh}^4 \left(\frac{\tilde{\upsilon}_{Rc}}{\sqrt{6}\,\alpha} \right) = \frac{\kappa^2 M^4 M_\star^2 \beta}{2\, m_{\rm Pl}^2 \lambda_N^2 (\sqrt{6}\,\alpha)^4}. \tag{8.4}$$

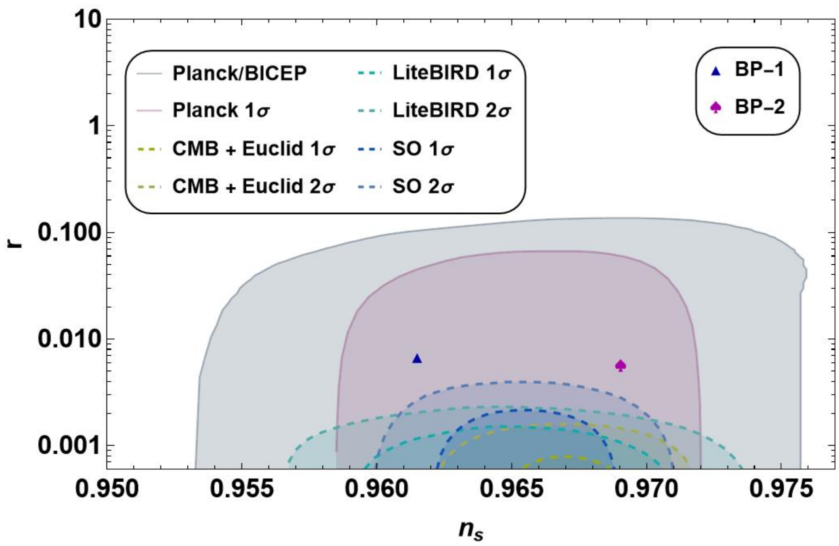

FIGURE 8: *Tensor-to-scalar ratio r vs. scalar spectral index n_s for the corresponding parameter sets given in table 3. The solid contours are the current Planck bounds [26], Planck/BICEP [25, 27, 28] and the dashed shaded region indicates the future proposed experiments (LiteBIRD, CMB-Euclid, Simons Observatory (SO)) [29–31].*

First we discuss what happens along the valley: as long as $\tilde{\upsilon}_R \lesssim \tilde{\upsilon}_{Rc}$, the effective mass square of $\tilde{\phi}$ stays negative. This gives rise to kind of tachyonic instability that leads to the large growth the curvature perturbations which consequently further enhance the scalar power spectrum at small scales of the universe. The collapse of large density fluctuations upon horizon reentry leads to PBH production. The presence of the linear term in the potential eq. (8.2) serves as not to keep the field $\tilde{\phi}$ exactly at $\tilde{\phi} = 0$ but makes it displaced. This also depends upon the sign of the coefficient of the linear term d. On one hand, this inflates away unnecessary topological defects and on the other hand also controls the peak of the power spectrum at small scales to rescues from PBH overproduction. We take $M \sim O(1)$ to avoid eternal inflation [21]. The parameter γ controls the amplitude of the plateau in the valley, the coupling λ_N defines the number of e-folds in the waterfall regime and κ will fix the amplitude of the power spectrum at the pivot scale $k_\star = 0.05\,{\rm Mpc}^{-1}$ that is $A_s \simeq 2.24 \times 10^{-9}$. We consider the model involving exponential α-attractor [89] in order to to get rid of the problem of initial conditions that we usually have in a standard hybrid scenario [19] (see [13, 21] for a detailed discussion of such initial conditions). Having considered these constraints, we define the BPs in table 3 for the potential in eq. (8.2).

The predicted n_s and r are shown in fig. 8. The field evolution from the pivot scale to the end of inflation using eq. (3.1) is shown in fig. 9. The scalar power spectrum eq. (3.7) with the variation of different model parameters is presented in fig. 10 along with the current and future experimental bounds as explained in section 5. The relevant PBH abundance is given

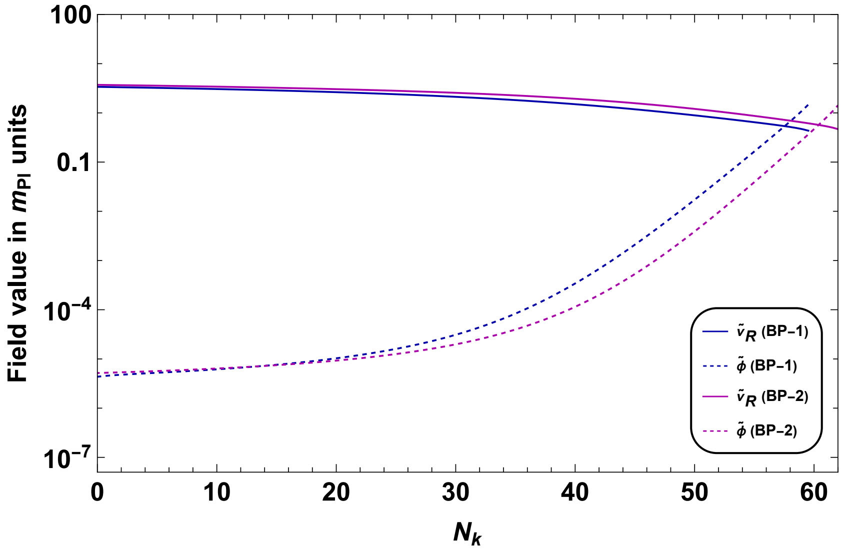

FIGURE 9: *Fields evolution with the number of e-folds from pivot scale to the end of inflation. We evaluate solving the full background eq. (3.1) using potential in eq. (8.2) for the benchmark points in table 3.*

Table 3: *Benchmark points for model−2 parameters*

Model	$M/m_{\mathbf{Pl}}$	$M_\star/m_{\mathbf{Pl}}$	$-(M'/m_{\mathbf{Pl}})^2$	β	λ_N	κ	$d/m_{\mathbf{Pl}}$
BP-1	1.352	1.0	−29.246	0.547	7.07×10^{-7}	1.7×10^{-6}	$-3.0{\times}10^{-6}$
BP-2	1.352	1.0	−29.246	0.600	6.26×10^{-7}	1.6×10^{-6}	$-2.8{\times}10^{-6}$

Model	γ	$\sqrt{\alpha}/m_{\mathbf{Pl}}$	$\tilde{\upsilon}_{Ri}/m_{\mathbf{Pl}}$	$\tilde{\phi}_i/m_{\mathbf{Pl}}$	N_k	n_s	r	$T_R/$**GeV**
BP-1	0.073	1	3.5	0	60	0.961	0.0068	9.8×10^8
BP-2	0.085	1	4.0	0	62	0.969	0.0056	9.2×10^8

in fig. 11 along with the present and future experimental bounds (see section 5.1 for details). The SGWB formed by the PBH and the variation of different model parameters along with the experimental sensitivities (explained in section 7) is given in fig. 12. It is important to note that the large value of the coupling β predicted in section 5.1 is now taking a natural value in the α-attractor scenario but the mass scale M is larger than the reduced Planck scale and is less than the Planck mass, see table 3.

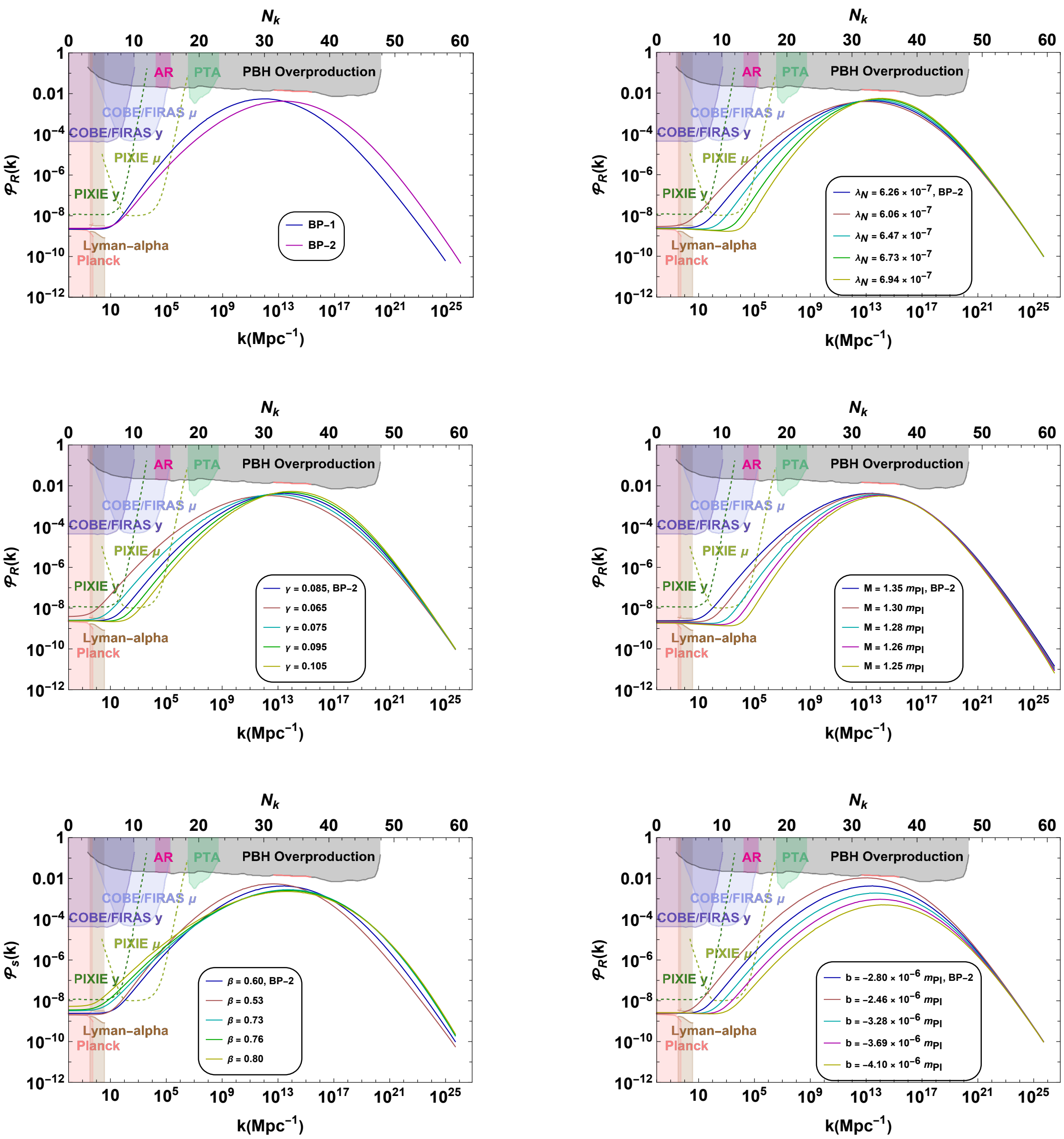

FIGURE 10: *Power spectrum by solving the exact linear scalar perturbation equations with the shaded region corresponding to the constraints from present (solid) and future (dashed) experiments. The corresponding set of parameters is given in table 3.*

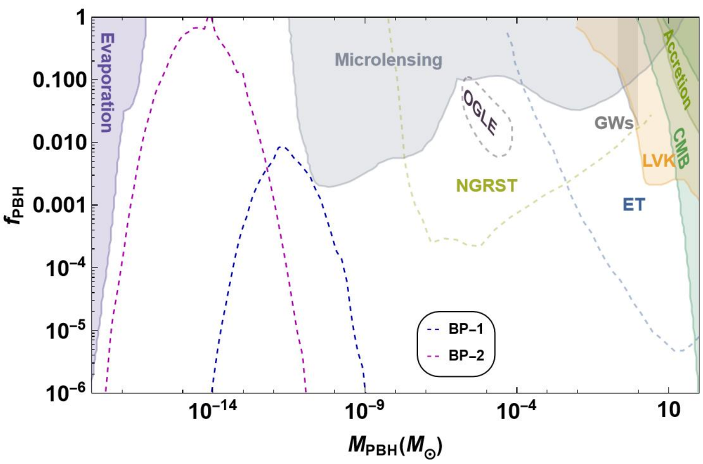

FIGURE 11: *PBH abundance given in eq. (6.2) for the BPs table 3. The shaded regions represent the observational constraints on the PBH abundance from various experiments, see the main text for the details. For BP-1, as we see it can be the entire DM candidate of the universe.*

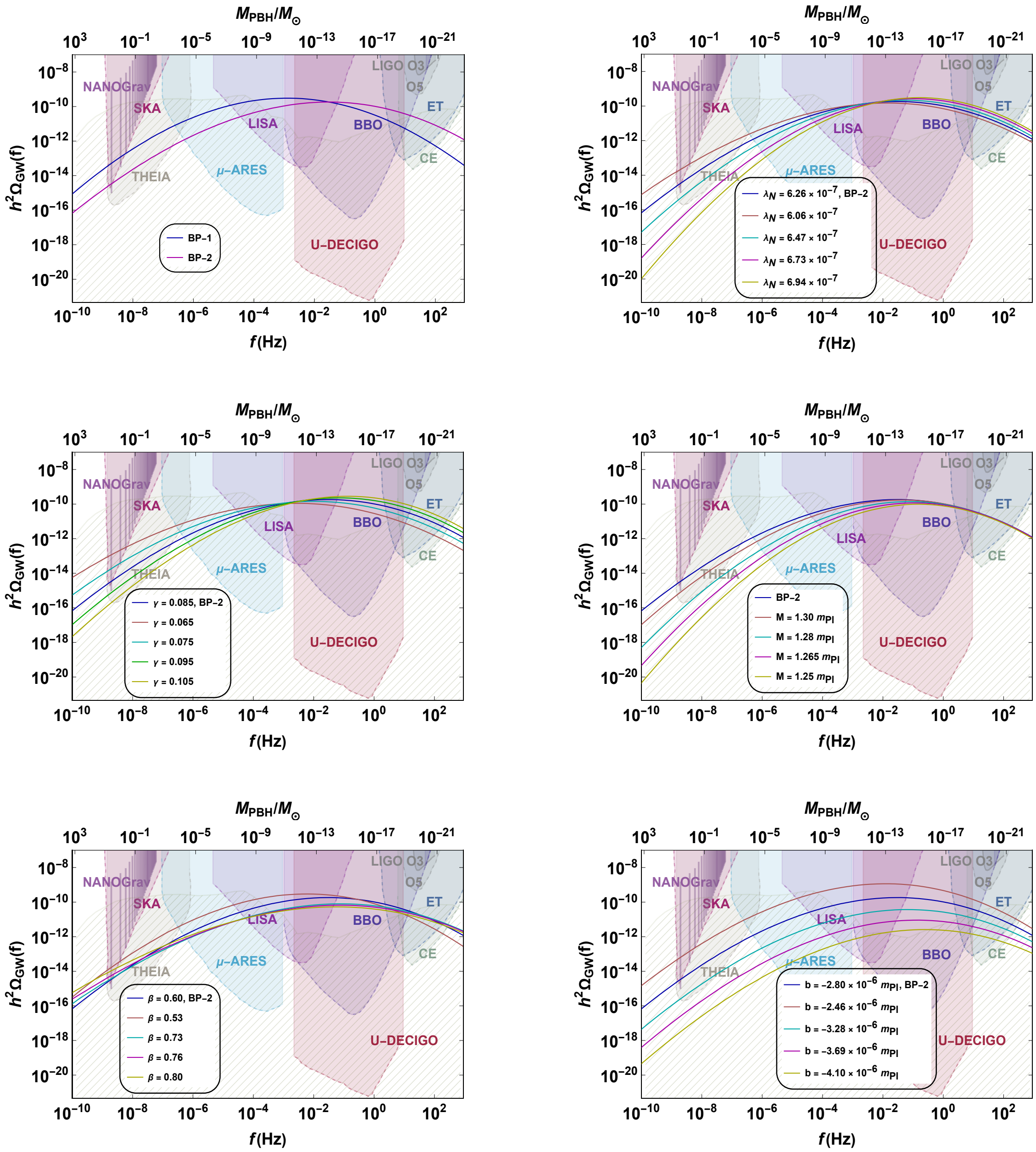

FIGURE 12: *The energy density of gravitational waves for eq. (7.1) for the BPs given in table 3. The colored shaded regions indicate the sensitivity curves of present (solid boundaries) LIGO O3 [86], NANOGrav [87] and future (dashed boundaries) LIGO O5, SKA [68], THEIA [69], LISA [70], μ-ARES [71], BBO [72], U-DECIGO [73, 74], CE [75] and ET [76] experiments. The hatched region shows the astrophysical background [88].*

9 Fine-tuning Estimate

The single-field inflationary models usually require a lot of fine-tuning of the parameters involved in the enhancement of the power spectrum at small scales [41]. However, in hybrid inflation due to the presence of another field, the amount of fine-tuning reduces significantly. The fine-tuning parameterization in terms of a quantity Δ_x is given by

$$\Delta_x = \text{Max}\left|\frac{\partial \ln P_s^{\text{Peak}}}{\partial \ln x}\right|. \tag{9.1}$$

Here, x is the underlying model parameter. The larger the Δ_x is, the larger the amount of required fine-tuning. Let us separately discuss each model we considered.

Model−1

In this framework, $x \in \{M, \phi_c, m_1\}$ in eq. (9.1). Evaluating numerically, fine-tuning estimates for toy model parameters eq. (2.1) are given in table 4. The maximum fine-tuning we obtain is 3, which is almost six orders of magnitude smaller than single-field inflation [90] and two orders of magnitude smaller than standard hybrid inflation previously explored [14]. We find

Table 4: *Fine-tuning (FT) estimate of model parameters for BP in table 1 with a peak of the spectrum around* 5×10^{-3}.

Δ_x	Δ_M	Δ_{ϕ_c}	Δ_{m_1}
FT	3	1	–

the fine-tuning estimate for m_1 is negligible.

Model−2

In this framework, $x \in \{M_1, \beta, \gamma, \lambda_N\}$ in eq. (9.1). Evaluating numerically, fine-tuning estimates for sneutrino theory parameters eq. (8.2) are given in table 5. The maximum fine-tuning we obtain is 8, which is almost five orders of magnitude smaller than single-field inflation [90] and one order of magnitude smaller than standard hybrid inflation [14].

Table 5: *Fine-tuning (FT) estimate of model parameters for BP−1 in table 3 with a peak of the spectrum around* 5×10^{-3}.

Δ_x	Δ_{M_1}	Δ_β	Δ_γ	Δ_{λ_N}
FT	8	3	1	4

10 Discussion and Conclusion

In summary, we presented two models of supersymmetric hybrid inflation (with sneutrino playing the role of the inflaton) and investigated the predictions of gravitational waves and primordial black holes generated during the waterfall transition which poses an added advantage of very mild fine-tuning unlike single field inflation [90]. We predict spectral index n_s to be 0.966 and the tensor-to-scalar ratio $r \simeq 10^{-11}$ for the first analysis based on the assumptions of the toy model. For the α-attractor case, ($n_s \simeq 0.961 - 0.969$) and ($r \simeq 0.0056 - 0.0068$). These predictions are consistent with the current Planck data and within the reach of next-generation CMB experiments like LiteBIRD, etc and also satisfy PBH as dark matter with detectable GW signal. The inflaton is the lightest singlet sneutrino, so it dominates the reheating after inflation. Using $\langle\phi\rangle = \sqrt{M'M}$, we find its mass to be $2(\lambda_N)_{11}M'M/M_*$. It decays mainly via the extended MSSM Yukawa coupling into slepton and Higgs or a lepton and Higgsino with a decay width given by $\Gamma_{\tilde{N}} = M_{\tilde{\mathrm{N}}}(Y_\nu^\dagger Y_\nu)_{11}/(4\pi)$. The decay of the singlet sneutrino after inflation is responsible for reheating the visible universe to a temperature $T_{\mathrm{RH}} \approx (90/(228.75\pi^2))^{1/4}\sqrt{\Gamma_{\tilde{N}} m_{\mathrm{P}}}$. Following this, the typical reheat temperature for both the models is around $10^7 - 10^8$ GeV suitable for non-thermal leptogenesis as shown in sections 5.1 and 8.

Particularly we were able to show a novel correlation between the mass of PBH, the peak in the GW spectrum, and the right-handed (s)neutrino mass in both the models. The salient features of our analysis are:

Model–1:

- We presented a toy model of hybrid inflation by adding the linear term that helps to avoid PBH overproduction. We derived an analytical expression for the power spectrum that fits very well with the numerical results up to a certain range of the coefficient of the linear term (see fig. 3).
- We achieved acceptable values for both spectral index ($n_s \simeq 0.966$) and tensor-to-scalar ratio ($r \simeq 10^{-11}$) satisfying PBH as the entire dark matter of the universe and detectable GW signals.
- We compared the toy model with the sneutrino canonical hybrid inflation potential where the inflation is driven by the sneutrino. The BPs are given in table 2. The model predicts a sub-Planckian mass parameter M, while the coupling between a gauge singlet and the waterfall field β is $O(10^2)$.
- Second-order tensor perturbations propagating as GWs are predicted with amplitude $\Omega_{\mathsf{GW}} h^2 \sim 10^{-9}$ and peak frequency $f \sim 0.1$ Hz by LISA and $\Omega_{\mathsf{GW}} h^2 \sim 10^{-11}$ and peak frequency of ~ 10 Hz in ET (see fig. 7). Production of PBH of mass around $10^{-13} M_\odot$ as the sole DM candidate in the universe is proposed. This novel DM candidate is also a signature of the sneutrino (see fig. 11).
- The fine-tuning for this model is almost $O(1)$ or smaller (see table 4) which shows its supremacy over the single field inflationary model.

Model–2:

- We modify the sneutrino potential by introducing an α-attractor transformation and see that the coupling β takes a naturally small value but the mass parameter M is larger (see table 3).
- We achieved acceptable values for both spectral index ($n_s \simeq 0.961 - 0.969$) and tensor-to-scalar ratio ($r \simeq 0.0056 - 0.0068$) satisfying PBH as dark matter and detectable GW signal.
- Second-order tensor perturbations propagating as GWs are predicted with amplitude $\Omega_{\mathsf{GW}} h^2 \sim 10^{-9}$ and peak frequency f ~ 0.1 Hz by LISA and $\Omega_{\mathsf{GW}} h^2 \sim 10^{-11}$ and peak frequency of ~ 10 Hz in ET in this model (see fig. 12). Production of PBH of mass around $10^{-13} M_\odot$ as the sole DM candidate in the universe is proposed. This novel DM candidate is also a signature of the sneutrino (see fig. 11).
- The fine-tuning for this model is almost $O(1)$ (see table 5) which is less than the hybrid inflation previously explored in the literature [13, 14].

Thus, we offer one potential way to test the origin of right-handed neutrino mass generation, which is currently inaccessible in colliders, using a GW detector.

As a future outlook, it could be interesting to study the impact of non-Gaussianities during the waterfall transition in the models studied as they impact the abundance of PBH formation rate, PBH clustering, and the amplitude of scalar-induced GW signals (see ref. [91, 92] for recent reviews). If some characteristic features of the GW spectral shapes encountered in this study are observed, one may look to target additional observations to distinguish between SUSY-mediated inflation and other scenarios. Particularly in sneutrino masses of TeV, these could be searched in experiments [93] at the particle physics laboratories. In this manner, we can complement

GW searches with laboratory searches in the same BSM parameter space. Gravitational wave astronomy with the planned global network of GW detectors aspires to achieve measurement precisions that are orders of magnitude better than the present day detectors. This new era of GW detectors worldwide will make the dream of testing fundamental BSM mechanisms, e.g. for supersymmetry physics, or neutrino physics of the universe and inflationary cosmology, a reality in the near future.

Acknowledgements

The authors thank Ahmad Moursy, Koushik Dutta, Konstantinos Dimopoulos, Rathul Raveendran, and Charalampos Tzerefos for the helpful comments. AA thanks Shahid Beheshti University Iran for the hospitality.

References

[1] D. Lynden-Bell, *Galactic nuclei as collapsed old quasars*, *Nature* **223** (1969) 690.

[2] J. Kormendy and D. Richstone, *Inward bound: The Search for supermassive black holes in galactic nuclei*, *Ann. Rev. Astron. Astrophys.* **33** (1995) 581.

[3] LIGO Scientific, Virgo collaboration, *Binary Black Hole Mergers in the first Advanced LIGO Observing Run*, *Phys. Rev. X* **6** (2016) 041015 [1606.04856].

[4] KAGRA, VIRGO, LIGO Scientific collaboration, *GWTC-3: Compact Binary Coalescences Observed by LIGO and Virgo during the Second Part of the Third Observing Run*, *Phys. Rev. X* **13** (2023) 041039 [2111.03606].

[5] S. Hawking, *Gravitationally collapsed objects of very low mass*, *Mon. Not. Roy. Astron. Soc.* **152** (1971) 75.

[6] B.J. Carr and S.W. Hawking, *Black holes in the early Universe*, *Mon. Not. Roy. Astron. Soc.* **168** (1974) 399.

[7] B.J. Carr, *The Primordial black hole mass spectrum*, *Astrophys. J.* **201** (1975) 1.

[8] A. Escrivà, F. Kuhnel and Y. Tada, *Primordial Black Holes*, 2211.05767.

[9] P.S. Cole, A.D. Gow, C.T. Byrnes and S.P. Patil, *Primordial black holes from single-field inflation: a fine-tuning audit*, *JCAP* **08** (2023) 031 [2304.01997].

[10] J. Garcia-Bellido, A.D. Linde and D. Wands, *Density perturbations and black hole formation in hybrid inflation*, *Phys. Rev. D* **54** (1996) 6040 [astro-ph/9605094].

[11] A.D. Linde, *Axions in inflationary cosmology*, *Phys. Lett. B* **259** (1991) 38.

[12] A.D. Linde, *Hybrid inflation*, *Phys. Rev. D* **49** (1994) 748 [astro-ph/9307002].

[13] A. Afzal and A. Ghoshal, *Primordial Black Holes and Scalar-induced Gravitational Waves in Radiative Hybrid Inflation*, 2402.06613.

[14] V.C. Spanos and I.D. Stamou, *Gravitational waves and primordial black holes from supersymmetric hybrid inflation*, *Phys. Rev. D* **104** (2021) 123537 [2108.05671].

[15] J.R. Ellis and S.K. Kang, *Sneutrino leptogenesis at the electroweak scale*, hep-ph/0505162.

[16] S. Clesse, *Hybrid inflation along waterfall trajectories*, *Phys. Rev. D* **83** (2011) 063518 [1006.4522].

[17] H. Kodama, K. Kohri and K. Nakayama, *On the waterfall behavior in hybrid inflation*, *Prog. Theor. Phys.* **126** (2011) 331 [1102.5612].

[18] D. Mulryne, S. Orani and A. Rajantie, *Non-Gaussianity from the hybrid potential*, *Phys. Rev. D* **84** (2011) 123527 [1107.4739].

[19] S. Clesse and J. García-Bellido, *Massive Primordial Black Holes from Hybrid Inflation as Dark Matter and the seeds of Galaxies*, *Phys. Rev. D* **92** (2015) 023524 [1501.07565].

[20] M. Kawasaki and Y. Tada, *Can massive primordial black holes be produced in mild waterfall hybrid inflation?*, *JCAP* **08** (2016) 041 [1512.03515].

[21] M. Braglia, A. Linde, R. Kallosh and F. Finelli, *Hybrid α-attractors, primordial black holes and gravitational wave backgrounds*, *JCAP* **04** (2023) 033 [2211.14262].

[22] A. Moursy and Q. Shafi, *Primordial monopoles, black holes and gravitational waves*, 2405.04397.

[23] Y. Cui and E.I. Sfakianakis, *Detectable gravitational wave signals from inflationary preheating*, *Phys. Lett. B* **840** (2023) 137825 [2112.00762].

[24] A. Chatterjee and A. Mazumdar, *Observable tensor-to-scalar ratio and secondary gravitational wave background*, *Phys. Rev. D* **97** (2018) 063517 [1708.07293].

[25] Planck collaboration, *Planck 2018 results. VI. Cosmological parameters*, *Astron. Astrophys.* **641** (2020) A6 [1807.06209].

[26] Planck collaboration, *Planck 2018 results. X. Constraints on inflation*, *Astron. Astrophys.* **641** (2020) A10 [1807.06211].

[27] BICEP, Keck collaboration, *Improved Constraints on Primordial Gravitational Waves using Planck, WMAP, and BICEP/Keck Observations through the 2018 Observing Season*, *Phys. Rev. Lett.* **127** (2021) 151301 [2110.00483].

[28] BICEP/Keck collaboration, *The Latest Constraints on Inflationary B-modes from the BICEP/Keck Telescopes*, in *56th Rencontres de Moriond on Cosmology*, 3, 2022 [2203.16556].

[29] R. Laureijs, J. Amiaux, S. Arduini, J.L. Augueres, J. Brinchmann, R. Cole et al., *Euclid definition study report*, 2011.

[30] Simons Observatory collaboration, *The Simons Observatory: Science goals and forecasts*, *JCAP* **02** (2019) 056 [1808.07445].

[31] LiteBIRD collaboration, *LiteBIRD: JAXA's new strategic L-class mission for all-sky surveys of cosmic microwave background polarization*, *Proc. SPIE Int. Soc. Opt. Eng.* **11443** (2020) 114432F [2101.12449].

[32] S. Clesse, B. Garbrecht and Y. Zhu, *Non-Gaussianities and Curvature Perturbations from Hybrid Inflation*, *Phys. Rev. D* **89** (2014) 063519 [1304.7042].

[33] C. Ringeval, *The exact numerical treatment of inflationary models*, *Lect. Notes Phys.* **738** (2008) 243 [astro-ph/0703486].

[34] S. Antusch, M. Bastero-Gil, S.F. King and Q. Shafi, *Sneutrino hybrid inflation in supergravity*, *Phys. Rev. D* **71** (2005) 083519 [hep-ph/0411298].

[35] S.F. King and Q. Shafi, *Minimal supersymmetric $SU(4) \times SU(2)_L \times SU(2)_R$*, *Phys. Lett. B* **422** (1998) 135 [hep-ph/9711288].

[36] G.R. Dvali, G. Lazarides and Q. Shafi, *Mu problem and hybrid inflation in supersymmetric $SU(2)_L x SU(2)_R x U(1)_(B-L)$*, *Phys. Lett. B* **424** (1998) 259 [hep-ph/9710314].

[37] I. Stamou, *Mechanisms for producing Primordial Black Holes from Inflationary Models Beyond Fine-Tuning*, 2404.14321.

[38] J. Chluba, A.L. Erickcek and I. Ben-Dayan, *Probing the inflaton: Small-scale power spectrum constraints from measurements of the CMB energy spectrum*, *Astrophys. J.* **758** (2012) 76 [1203.2681].

[39] D.J. Fixsen, E.S. Cheng, J.M. Gales, J.C. Mather, R.A. Shafer and E.L. Wright, *The Cosmic Microwave Background spectrum from the full COBE FIRAS data set*, *Astrophys. J.* **473** (1996) 576 [astro-ph/9605054].

[40] A. Kogut, D. Fixsen, D. Chuss, J. Dotson, E. Dwek, M. Halpern et al., *The primordial inflation explorer (pixie): a nulling polarimeter for cosmic microwave background observations*, *Journal of Cosmology and Astroparticle Physics* **2011** (2011) 025–025.

[41] G. Ballesteros and M. Taoso, *Primordial black hole dark matter from single field inflation*, *Phys. Rev. D* **97** (2018) 023501 [1709.05565].

[42] H. Motohashi and W. Hu, *Primordial Black Holes and Slow-Roll Violation*, *Phys. Rev. D* **96** (2017) 063503 [1706.06784].

[43] I. Musco, V. De Luca, G. Franciolini and A. Riotto, *Threshold for primordial black holes. II. A simple analytic prescription*, *Phys. Rev. D* **103** (2021) 063538 [2011.03014].

[44] A. Escrivà, C. Germani and R.K. Sheth, *Analytical thresholds for black hole formation in general cosmological backgrounds*, *JCAP* **01** (2021) 030 [2007.05564].

[45] A. Escrivà, C. Germani and R.K. Sheth, *Universal threshold for primordial black hole formation*, *Phys. Rev. D* **101** (2020) 044022 [1907.13311].

[46] I. Musco, *Threshold for primordial black holes: Dependence on the shape of the cosmological perturbations*, *Phys. Rev. D* **100** (2019) 123524 [1809.02127].

[47] A.M. Green and B.J. Kavanagh, *Primordial Black Holes as a dark matter candidate*, *J. Phys. G* **48** (2021) 043001 [2007.10722].

[48] S. Clark, B. Dutta, Y. Gao, L.E. Strigari and S. Watson, *Planck Constraint on Relic Primordial Black Holes*, *Phys. Rev. D* **95** (2017) 083006 [1612.07738].

[49] S. Mittal, A. Ray, G. Kulkarni and B. Dasgupta, *Constraining primordial black holes as dark matter using the global 21-cm signal with X-ray heating and excess radio background*, *JCAP* **03** (2022) 030 [2107.02190].

[50] R. Laha, J.B. Muñoz and T.R. Slatyer, *INTEGRAL constraints on primordial black holes and particle dark matter*, *Phys. Rev. D* **101** (2020) 123514 [2004.00627].

[51] J. Berteaud, F. Calore, J. Iguaz, P.D. Serpico and T. Siegert, *Strong constraints on primordial black hole dark matter from 16 years of INTEGRAL/SPI observations*, *Phys. Rev. D* **106** (2022) 023030 [2202.07483].

[52] M. Boudaud and M. Cirelli, *Voyager 1 $e^{\pm}$ Further Constrain Primordial Black Holes as Dark Matter*, *Phys. Rev. Lett.* **122** (2019) 041104 [1807.03075].

[53] W. DeRocco and P.W. Graham, *Constraining Primordial Black Hole Abundance with the Galactic 511 keV Line*, *Phys. Rev. Lett.* **123** (2019) 251102 [1906.07740].

[54] B.J. Carr, K. Kohri, Y. Sendouda and J. Yokoyama, *New cosmological constraints on primordial black holes*, *Phys. Rev. D* **81** (2010) 104019 [0912.5297].

[55] H. Niikura et al., *Microlensing constraints on primordial black holes with Subaru/HSC Andromeda observations*, *Nature Astron.* **3** (2019) 524 [1701.02151].

[56] EROS-2 collaboration, *Limits on the Macho Content of the Galactic Halo from the EROS-2 Survey of the Magellanic Clouds*, *Astron. Astrophys.* **469** (2007) 387 [astro-ph/0607207].

[57] H. Niikura, M. Takada, S. Yokoyama, T. Sumi and S. Masaki, *Constraints on Earth-mass primordial black holes from OGLE 5-year microlensing events*, *Phys. Rev. D* **99** (2019) 083503 [1901.07120].

[58] M. Oguri, J.M. Diego, N. Kaiser, P.L. Kelly and T. Broadhurst, *Understanding caustic crossings in giant arcs: characteristic scales, event rates, and constraints on compact dark matter*, *Phys. Rev. D* **97** (2018) 023518 [1710.00148].

[59] P.D. Serpico, V. Poulin, D. Inman and K. Kohri, *Cosmic microwave background bounds on primordial black holes including dark matter halo accretion*, *Phys. Rev. Res.* **2** (2020) 023204 [2002.10771].

[60] G. Franciolini, I. Musco, P. Pani and A. Urbano, *From inflation to black hole mergers and back again: Gravitational-wave data-driven constraints on inflationary scenarios with a first-principle model of primordial black holes across the QCD epoch*, *Phys. Rev. D* **106** (2022) 123526 [2209.05959].

[61] B.J. Kavanagh, D. Gaggero and G. Bertone, *Merger rate of a subdominant population of primordial black holes*, *Phys. Rev. D* **98** (2018) 023536 [1805.09034].

[62] V. De Luca, G. Franciolini, P. Pani and A. Riotto, *Bayesian Evidence for Both Astrophysical and Primordial Black Holes: Mapping the GWTC-2 Catalog to Third-Generation Detectors*, *JCAP* **05** (2021) 003 [2102.03809].

[63] V. De Luca, G. Franciolini, P. Pani and A. Riotto, *The minimum testable abundance of primordial black holes at future gravitational-wave detectors*, *JCAP* **11** (2021) 039 [2106.13769].

[64] G. Franciolini, F. Iacovelli, M. Mancarella, M. Maggiore, P. Pani and A. Riotto, *Searching for primordial black holes with the Einstein Telescope: Impact of design and systematics*, *Phys. Rev. D* **108** (2023) 043506 [2304.03160].

[65] W. DeRocco, E. Frangipane, N. Hamer, S. Profumo and N. Smyth, *Rogue worlds meet the dark side: revealing terrestrial-mass primordial black holes with the Nancy Grace Roman Space Telescope*, 2311.00751.

[66] J.R. Espinosa, D. Racco and A. Riotto, *A Cosmological Signature of the SM Higgs Instability: Gravitational Waves*, *JCAP* **09** (2018) 012 [1804.07732].

[67] V. De Luca, G. Franciolini and A. Riotto, *NANOGrav Data Hints at Primordial Black Holes as Dark Matter*, *Phys. Rev. Lett.* **126** (2021) 041303 [2009.08268].

[68] R. Smits, M. Kramer, B. Stappers, D.R. Lorimer, J. Cordes and A. Faulkner, *Pulsar searches and timing with the square kilometre array*, *Astron. Astrophys.* **493** (2009) 1161 [0811.0211].

[69] J. Garcia-Bellido, H. Murayama and G. White, *Exploring the early Universe with Gaia and Theia*, *JCAP* **12** (2021) 023 [2104.04778].

[70] J. Baker et al., *The Laser Interferometer Space Antenna: Unveiling the Millihertz Gravitational Wave Sky*, 1907.06482.

[71] A. Sesana et al., *Unveiling the gravitational universe at μ-Hz frequencies*, *Exper. Astron.* **51** (2021) 1333 [1908.11391].

[72] V. Corbin and N.J. Cornish, *Detecting the cosmic gravitational wave background with the big bang observer*, *Class. Quant. Grav.* **23** (2006) 2435 [gr-qc/0512039].

[73] K. Yagi and N. Seto, *Detector configuration of DECIGO/BBO and identification of cosmological neutron-star binaries*, *Phys. Rev. D* **83** (2011) 044011 [1101.3940].

[74] S. Kawamura et al., *Current status of space gravitational wave antenna DECIGO and B-DECIGO*, *PTEP* **2021** (2021) 05A105 [2006.13545].

[75] D. Reitze et al., *Cosmic Explorer: The U.S. Contribution to Gravitational-Wave Astronomy beyond LIGO*, *Bull. Am. Astron. Soc.* **51** (2019) 035 [1907.04833].

[76] M. Punturo et al., *The Einstein Telescope: A third-generation gravitational wave observatory*, *Class. Quant. Grav.* **27** (2010) 194002.

[77] LIGO Scientific, Virgo collaboration, *GW170814: A Three-Detector Observation of Gravitational Waves from a Binary Black Hole Coalescence*, *Phys. Rev. Lett.* **119** (2017) 141101 [1709.09660].

[78] LIGO Scientific, Virgo collaboration, *GWTC-1: A Gravitational-Wave Transient Catalog of Compact Binary Mergers Observed by LIGO and Virgo during the First and Second Observing Runs*, *Phys. Rev. X* **9** (2019) 031040 [1811.12907].

[79] LIGO Scientific, Virgo collaboration, *GW170817: Observation of Gravitational Waves from a Binary Neutron Star Inspiral*, *Phys. Rev. Lett.* **119** (2017) 161101 [1710.05832].

[80] C. Cutler and J. Harms, *BBO and the neutron-star-binary subtraction problem*, *Phys. Rev. D* **73** (2006) 042001 [gr-qc/0511092].

[81] T. Regimbau, M. Evans, N. Christensen, E. Katsavounidis, B. Sathyaprakash and S. Vitale, *Digging deeper: Observing primordial gravitational waves below the binary black hole produced stochastic background*, *Phys. Rev. Lett.* **118** (2017) 151105 [1611.08943].

[82] C.J. Moore, R.H. Cole and C.P.L. Berry, *Gravitational-wave sensitivity curves*, *Class. Quant. Grav.* **32** (2015) 015014 [1408.0740].

[83] D.I. Kosenko and K.A. Postnov, *On the gravitational wave noise from unresolved extragalactic binaries*, *Astron. Astrophys.* **336** (1998) 786 [astro-ph/9801032].

[84] M.R. Adams and N.J. Cornish, *Detecting a Stochastic Gravitational Wave Background in the presence of a Galactic Foreground and Instrument Noise*, *Phys. Rev. D* **89** (2014) 022001 [1307.4116].

[85] X.-J. Zhu, E.J. Howell, D.G. Blair and Z.-H. Zhu, *On the gravitational wave background from compact binary coalescences in the band of ground-based interferometers*, *Mon. Not. Roy. Astron. Soc.* **431** (2013) 882 [1209.0595].

[86] KAGRA, Virgo, LIGO Scientific collaboration, *Upper limits on the isotropic gravitational-wave background from Advanced LIGO and Advanced Virgo's third observing run*, *Phys. Rev. D* **104** (2021) 022004 [2101.12130].

[87] NANOGrav collaboration, *The NANOGrav 15 yr Data Set: Evidence for a Gravitational-wave Background*, *Astrophys. J. Lett.* **951** (2023) L8 [2306.16213].

[88] A. Ghoshal and A. Strumia, *Traversing a kinetic pole during inflation: primordial black holes and gravitational waves*, 2023.

[89] R. Kallosh and A. Linde, *Hybrid cosmological attractors*, *Phys. Rev. D* **106** (2022) 023522 [2204.02425].

[90] I.D. Stamou, *Mechanisms of producing primordial black holes by breaking the* $SU(2,1)/SU(2) \times U(1)$ *symmetry*, *Phys. Rev. D* **103** (2021) 083512 [2104.08654].

[91] G. Domènech, *Scalar Induced Gravitational Waves Review*, *Universe* **7** (2021) 398 [2109.01398].

[92] S. Pi, *Non-Gaussianities in primordial black hole formation and induced gravitational waves*, 2404.06151.

[93] Particle Data Group collaboration, *Review of Particle Physics*, *PTEP* **2022** (2022) 083C01.